PROCEEDINGS OF SCIENCE

QCD phase diagram in a magnetic background

Massimo D'Elia,[a] **Lorenzo Maio,**[a,*] **Francesco Sanfilippo**[b] **and Alfredo Stanzione**[c]

[a] *Dipartimento di Fisica dell'Università di Pisa and INFN - Sezione di Pisa, Largo Pontecorvo 3, I-56127, Pisa, Italy*

[b] *INFN - Sezione di Roma Tre, Via della Vasca Navale 84, I-00146, Rome, Italy*

[c] *SISSA, Via Bonomea 265, I-34136, Trieste, Italy*

E-mail: massimo.delia@unipi.it, lorenzo.maio@phd.unipi.it, francesco.sanfilippo@infn.it, alfredo.stanzione@sissa.it

We discuss the QCD phase diagram in the presence of a strong background magnetic field. We provide numerical evidence, based on lattice simulations of QCD with $2+1$ flavours and physical quark masses, for a crossover transition at $eB = 4$ GeV^2 (with a pseudo-critical temperature $T_c = (98 \pm 3)$ MeV) and for a first order phase transition at $eB = 9$ GeV^2 (where the measured critical temperature is $T_c = (63 \pm 5)$ MeV). We conclude that the critical endpoint is located at $eB = eB_{CEP}$ and $T = T_{CEP}$, where 4 GeV^2 $< eB_{CEP} <$ 9 GeV^2 and 63 MeV$< T_{CEP} <$ 98 MeV.

The 39th International Symposium on Lattice Field Theory (Lattice2022), 8-13 August, 2022 Bonn, Germany

*Speaker

© Copyright owned by the author(s) under the terms of the Creative Commons Attribution-NonCommercial-NoDerivatives 4.0 International License (CC BY-NC-ND 4.0).

PoS(LATTICE2022)184

1. Introduction

QCD properties in a strong magnetic background have been widely studied in the last years [1, 2]. The interest on such a topic is justified by the wide number of contexts in which strong magnetic fields arise, and by their theoretical and phenomenological relevance: Early Universe [3], heavy ion scattering experiments [4] and magnetars [5] are the physical systems that can be found in such conditions, and whose understanding could be improved studying how QCD behaves in strong magnetic fields.

Magnetic fields are known to affect confinement and chiral properties already at vanishing temperature [6–9], then it is natural to expect effects on the chiral and deconfining transitions at high temperatures. Thermal QCD at the physical point in a magnetic background has already been studied, up to intensities of $eB = 3.82$ GeV^2 [10, 11], and a proposal for a phase diagram where a critical line appears for $eB \gtrsim 10$ GeV^2 was formulated in Ref. [11]. In this work [12], we simulate $N_f = 2 + 1$ QCD with physical quark masses, probing the phase diagram at previously unexplored field intensities, namely $eB = 4$ GeV^2 and 9 GeV^2, finding that a first order phase transition actually takes place in the stronger magnetic background. Moreover, we observe that the critical temperature in the stronger magnetic background is quite lower than the previously predicted value. In this work, we provide a new sketch of the QCD phase diagram in the presence of a strong background magnetic field, which features the currently most precise determination of the critical end point position.

This paper is organized as follows, in Sections 2 and 3 we discuss the setup of lattice simulations, and introduce the measured observables; in Section 4 and 5, we present our findings on the transition temperature and on the transition nature; in Section 6 the confinement properties of the two phases are discussed; and, finally, in Section 7 we sum up all the results discussed in the paper and show the updated phase diagram.

2. Lattice setup

We simulated $N_f = 2 + 1$ QCD using tree-level improved Symanzik pure gauge action and stout improved staggered fermions with rooting technique, the partition function being

$$Z = \int d[U] e^{-S^{lat}}. \tag{1}$$

In Equation (1), U are the link variables, and

$$S^{lat}[U] = -\frac{\beta}{3} \sum_i \sum_{\mu<\nu} \left[\frac{5}{3} \mathrm{ReTr}\left(P_{i;\mu\nu}\right) - \frac{1}{6} \mathrm{ReTr}\left(R_{i;\mu\nu}\right) \right] - \sum_{f=u,d,s} \log \left\{ \det \left[M_f^{stag} \right]^{\frac{1}{4}} \right\}, \tag{2}$$

where $P_{i;\mu\nu}$ and $R_{i;\mu\nu}$ are, respectively, the 1×1 and 2×2 Wilson loops starting at the lattice site i and lying on the $\mu\nu$ plane, and

$$M_f^{stag}{}_{i,j} = \hat{m}_f \, \delta_{i,j} + \sum_{\mu=1}^{4} \frac{\eta_{i;\mu}}{2} \left[U^{(2)}_{i;\mu} \, \delta_{i,j-\hat{\mu}} + U^{(2)\dagger}_{i-\hat{\mu};\mu} \, \delta_{i,j+\hat{\mu}} \right], \tag{3}$$

with $\hat{m}_f$ the bare f-quark mass, $\eta_{i;\mu}$ the staggered quark phases, and $U^{(2)}_{i;\mu}$ the doubly stouted gauge link connecting the site i to the site $i + \hat{\mu}$.

PoS(LATTICE2022)184

We introduced the magnetic field by inserting an additional $U(1)$ phase to the link variables in the quark part of the action:

$$U^{(2)}_{i;\mu} \to U^{(2)\,f}_{i;\mu} = u^f_{i;\mu}\, U^{(2)}_{i;\mu}, \tag{4}$$

where, in order to obtain a z-oriented uniform magnetic field, we set to 1 all the abelian phases but the following

$$u^f_{i;y} = e^{i\,a^2 q_f B\, i_x}, \qquad u^f_{i;x}\Big|_{i_x = L_x} = e^{-i\,a^2 q_f L_x B\, i_y}, \tag{5}$$

being a the lattice spacing, i_μ the μ cartesian component of the i-th point, in lattice units, L_μ the lattice extent in the same direction, q_f the f quark electric charge, and B the magnetic field intensity. To avoid ambiguity in the phase acquired by a charged particle moving through a closed path, we quantized the magnetic field, introducing the quantum number $b_z \in \mathbb{Z}$,

$$q_f B = \frac{2\pi b_z}{a^2 L_x L_y} \implies eB = \frac{6\pi b_z}{a^2 L_x L_y}. \tag{6}$$

The right hand side of Equation (6) is the magnetic field intensity felt by the smallest quark charge $q_f = e/3$. Finally, to avoid periodicity effects in Equation (5), it is advisable to choose b_z such that

$$2b_z \ll L_x L_y. \tag{7}$$

We performed measurements of chiral symmetry and confinement relevant observables on three different lattice spacings, namely $a = 0.057$, 0.086 and 0.114 fm. The scale has been set using tables provided in Refs. [13–15], and interpolated data. For all the lattice spacings, we simulated different temperatures in a fixed-scale approach, by varying the number of sites in the compactified time direction, L_t, exploiting the relation $T^{-1} = aL_t$. Then, by choosing the same physical spatial volume for all the lattice spacings simulations, $\sim (2.75\text{ fm})^3$, we were able to simulate $eB = 4$ and 9 GeV^2 magnetic fields using the same value of b_z for every lattice spacing: respectively $b_z = 41$ and 93. The fixed scale approach was used for all the simulations but those aimed to study the nature of the transition. Details on the latter are available in Section 5.

3. Observables

In the absence of external magnetic fields, at the critical temperature, $T_C \simeq 160$ MeV, QCD goes through a crossover transition to an approximately chiral restored and deconfined phase. We talk about approximate symmetry and confinement because, in full QCD with non vanishing quark masses, none of these properties is well defined. However, the observables related to both chiral symmetry and confinement notably change across the crossover, and therefore they can be used to locate the transition.

To study the chiral symmetry behavior across the crossover, we studied the change in the chiral condensate, $\langle\bar\psi\psi\rangle_f$, which can be computed on the lattice as

$$\langle\bar\psi\psi\rangle_f = \frac{1}{4\,a^3 L_s^3 L_t}\left\langle \mathrm{Tr}\left(M^f_{st}\right)^{-1}\right\rangle. \tag{8}$$

The bare definition in Equation (8) brings scale dependent counter terms, which can be canceled by the subtraction of the vacuum expectation value [16]. Moreover, we studied the effects on the

PoS(LATTICE2022)184

lightest quarks, for which the chiral symmetry is a better approximation. Thus, we studied the following renormalized quantity

$$\frac{\Sigma_l^r(B,T)}{\Sigma_l^r(B,T=0)}, \tag{9}$$

where

$$\Sigma_l^r(B,T) = C(a) \sum_{f=u,d} \langle\overline{\psi}\psi\rangle_f(B,T) - \langle\overline{\psi}\psi\rangle_f(B=0,T=0) \tag{10}$$

and $C(a)$ is a scale dependent multiplicative renormalization constant, which cancel in the ratio of Equation (9), because of the fixed scale scheme we used.

A genuine transition is expected to be signaled, on finite volume lattice simulations, by a peculiar scaling behavior of the chiral susceptibility, $\chi(T)$. In detail, the susceptibility is expected to obey the scaling law

$$\chi(T;L_s) = L_s^{\gamma/\nu}\phi\left((T-T_c)L_s^{1/\nu}\right), \tag{11}$$

where ϕ is an unknown scaling function, and ν and γ are the critical indices, whose values are, respectively, $\frac{1}{3}$ and 1 for a first order phase transition. T_c is the same for every quark flavor, thus we restricted our analysis on the susceptibility to χ_u, which is expected to show the best signal-to-noise ratio, because of the low mass and the big electric charge. Moreover, since our goal was to only infer the nature of the transition from the study of this observable, we focused only on the bare disconnected part of the up-quark chiral susceptibility, namely

$$\chi_u^{disc} = \frac{1}{L_s L_t}\left[\langle\overline{\psi}\psi^2\rangle_u - \langle\overline{\psi}\psi\rangle_u{}^2\right], \tag{12}$$

which is expected to diverge itself at a genuine transition.

On the confinement side, we studied, around the transition, the behavior of the string tension, σ, i.e. the slope of the linear rising quark–anti-quark pair potential in the large distances limit. The potential can be studied on the lattice through Wilson loops, thanks to the relation

$$aV(a\vec{n}) = \lim_{an_t\to\infty} \frac{\langle \operatorname{Tr} W(a\vec{n}, an_t)\rangle}{\langle \operatorname{Tr} W(a\vec{n}, a(n_t+1))\rangle} \tag{13}$$

where $a\vec{n}$ is the spatial extent of the Wilson loop, n_t the temporal extent, and $V(a\vec{n})$ is the potential of a static quark–anti-quark pair at physical distance $a\vec{n}$. To take the limit $an_t \to \infty$, we performed a constant fit on the plateau of the right hand side of Equation (13) appearing at high values of n_t. The use of such a prescription in a finite temperature framework is made possible by the low values reached by T_c (cfr. Section 4), which, in turn, imply large temporal extensions around the transition in the fixed scale approach.

4. The transition temperature

We measured the chiral observable of Equation (9) for different values of the temperature and the lattice cut-off, see Figure 1. We can observe, in both panels, two regions characterized by two different values of the chiral condensate: high values in the cold region, and low values in the hot one. Between these two regimes, the transition temperature clearly moves towards lower values as

PoS(LATTICE2022)184

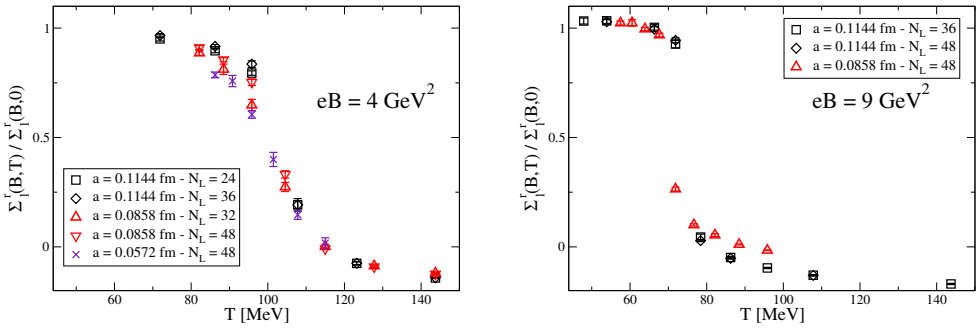

Figure 1: *(left)* Chiral condensate measures at $eB = 4$ GeV^2, for different temperatures, volumes and lattice spacings. A smooth crossover transition can be observed between the cold phase and the hot one. *(right)* Chiral condensate measures at $eB = 9$ GeV^2, for different temperatures, volumes and lattice spacings. A sharp jump is observed between the two phases, as expected for a real phase transition.

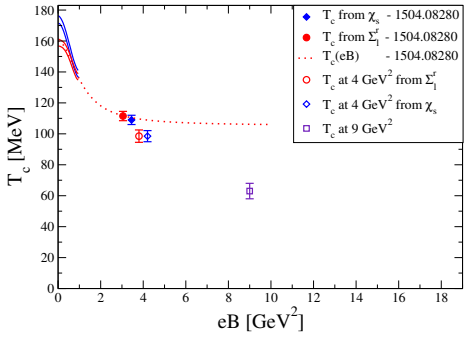

Figure 2: Critical temperatures measured in this work, compared with previous results and prediction from [11]. A big, unpredicted drop in the transition temperature is found at $eB = 9$ GeV^2.

the magnetic field increases. In the $eB = 4$ GeV^2 case (the left plot in Fig. 1), where the transition is smooth enough, we evaluate it as the abscissa of the inflection point of the best fit curve. To estimate the systematic error, we used different fitting functions and compared the results for T_c. In the $eB = 9$ GeV^2 plot (the right one), the transition region is too sharp, with a gap appearing between the two phases. We then locate T_c in the center of the gap region and assign the gap width as the confidence level.

In Figure 2 we plot our results for the continuum extrapolated values of $T_c(B)$, in comparison with the estimates and predictions provided in Ref. [11]. A steady, unexpected drop in the transition temperature can be observed in the $eB = 9$ GeV^2 case, whose value ranges down to 63 MeV. If $T_c(B)$ hits the 0 or not, for some finite $B = B_0$ value, is still an open question.

5. The transition nature

The steep drop in chiral condensate between the cold and the hot phases shown in the $eB = 9$ GeV^2 in Figure 1, signals the possibility for the transition to be a first order. To infer its nature, a finite size scaling (FSS) analysis of the chiral susceptibility is needed. Because of the fixed scale approach to thermal simulations we used, presented in Section 2, a FSS analysis on the physical line is hardly feasible.

PoS(LATTICE2022)184

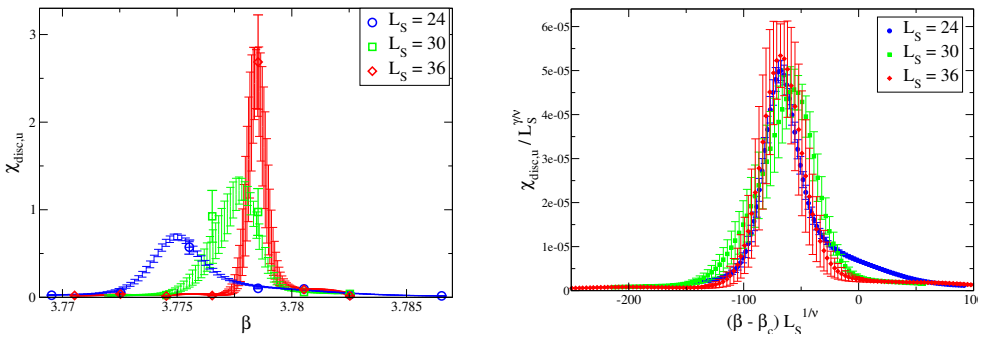

Figure 3: *(left)* Multi histogram interpolation in β of the chiral susceptibility, for three different lattice sizes. Big bold points represent the measured values, while thin lines are the interpolated measures. *(right)* Curves scaling according to first order transition critical exponents: $\gamma = 1$ and $\nu = 1/3$. The curves collapsing onto each other within the errors are a strong evidence for the first order nature of the transition.

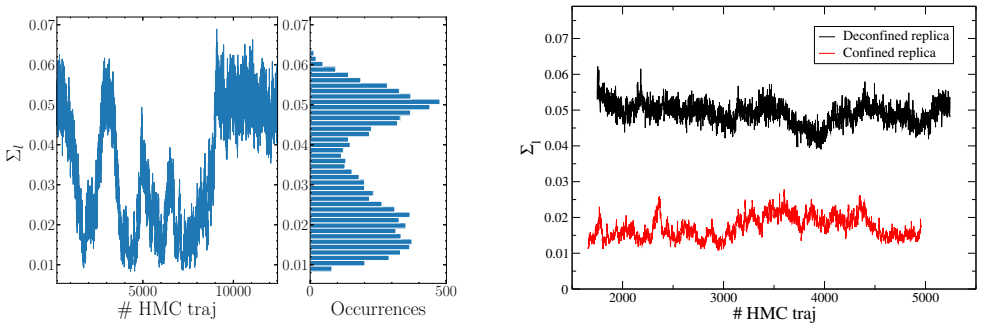

Figure 4: *(left)* Chiral condensate MC history of the simulation performed next to pseudo-critical β in the 24^3 lattice. The histogram clearly shows a double peaked distribution, as expected for a real phase transition. *(right)* Chiral condensate MC history for two $\beta = 3.778$ simulations in the 36^3 lattice, starting from configurations in the two different phases. Because of the larger volume the tunneling of one history into the other is less probable.

To get around this problem, we adopted a different strategy: for a new set of dedicated simulations, using as starting configuration the nearest-to-the-transition, we performed a temperature scan keeping N_t fixed and varying only the inverse gauge coupling β, until the phase transition takes place. Such a procedure allows us to easily perform a multi histogram interpolation, which permits a continuous scan in beta between the actually measured points. The measurements of the disconnected chiral susceptibility (12) for the up quark in three different lattice sizes, L_s, are presented in Figure 3. The peak height in the left panel strongly depends on the volume, as expected for a real phase transition. Rescaling the measurements according to (11) using the first order transition critical exponents, all the curves nicely collapse onto each other within the errors, providing a strong evidence for a first order phase transition happening.

Other convincing signals for a real phase transition can be found looking at the Monte Carlo (MC) histories of the chiral condensate, in the set of simulations dedicated to the FSS analysis. In the left panel of Figure 4, the MC history of the bare chiral condensate can be observed. It refers to one of the simulations performed using a β next to the chiral susceptibility peak in a 24^3 lattice volume. The numerous jumps between the two different equilibrium states are a typical real phase

PoS(LATTICE2022)184

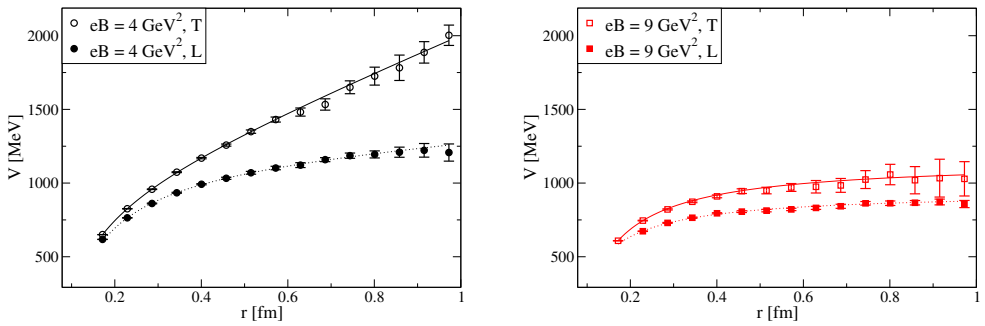

Figure 5: Static quark–anti-quark pair potentials (13), measured on the finest lattice, at the temperature of 86 MeV, in the transverse (T) and longitudinal (L) directions. (*left*) $eB = 4$ GeV^2 measurements: anisotropic confinement is found, with a drop of the string tension in the L direction and an enhancement in the T direction. (*right*) $eB = 9$ GeV^2 measurements: deconfinement is found in both the L and the T directions, with anisotropic Coulomb-like potential.

transition footprint. This kind of fluctuations become far less probable in the thermodynamic limit, where the barrier between the two meta-stable equilibrium states diverges. Such an effect can be observed in the right panel of Figure 4, where we show two simulations performed in a 36^3 lattice volume, with the same β (next to the critical one) but different starting points. Both the simulations oscillate around the nearest meta-stable equilibrium point, without tunneling to each other (at least, for the duration of our simulation).

6. Confinement in the two phases

We studied the static quark–anti-quark potential for two different ensembles at the same temperature, in the two background magnetic fields. We performed the measures on a $48^3 \times 40$ lattice, setting the temperature to $T \simeq 86$ MeV, which corresponds to the chiral-broken phase for the $eB = 4$ GeV^2 background and to the chiral-restored phase for the $eB = 9$ GeV^2 (cfr. the two panels in Figure 1).

In Figure 5 we show the results for the measurements of the observable defined in Equation (13) along two different spatial directions for each magnetic field. A drop of the static potential can be seen along the longitudinal direction with respect to the transversal one in both the cases, even if this effect is less evident in the right panel, representing the results for $eB = 9$ GeV^2. To measure the string tension, we fit the Cornell ansatz

$$V(r) = V_0 + \frac{\alpha}{r} + \sigma r, \tag{14}$$

to the data shown in Figure 5, and extract the best fit value for σ. We get a finite string tension in both the longitudinal and the transversal directions for the $eB = 4$ GeV^2, while a vanishing value for σ is returned by this procedure in the $eB = 9$ GeV^2 case. Thus, we conclude that the left panel plot exhibits confinement, while the right panel one exhibits deconfinement.

PoS(LATTICE2022)184

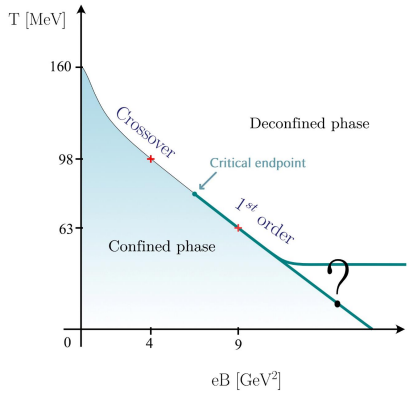

Figure 6: The updated QCD phase diagram in the presence of a constant, uniform, background magnetic field. The low magnetic field part is unaltered from previous proposal. Red crosses point to transition temperature measures performed in this work, the thin line represents where crossover transition happens, while the bold one is the critical line. The critical endpoint position is a guess, it is surely placed on the line connecting the two red crosses. The asymptotic behavior of the critical temperature in magnetic field is still unexplored.

7. Conclusions

We performed simulations of 2+1 flavors QCD with unprecedented strong background magnetic fields, namely $eB = 4$ and 9 GeV^2. We found an unforeseen drop in the transition temperature for growing magnetic fields, which, in the strongest background explored, is suppressed by a factor of ~ 2.5, with respect to its value at $B = 0$. Moreover we observe, as expected, a crossover transition in the $eB = 4$ GeV^2 case, while a first order phase transition occurs in the $eB = 9$ GeV^2 case. Thus the end point of the critical line must lie in (T_{cep}, eB_{cep}), where 63 MeV$< T_{cep} <$ 98 MeV and 4 GeV$^2 < eB_{cep} <$ 9 GeV^2. Moreover, we studied the static quark–anti-quark pair potential in both the phases, still observing confinement in the cold, chiral borken phase and deconfinement in the hot, chiral restored phase.

Our findings are summarized in Fig. 6, where they are reported within an updated phase diagram of the QCD in the presence of a background magnetic field. The question mark refers to the critical temperature behavior as a function of the external magnetic field. A drop to 0 for $T_c(eB)$ is not expected for finite values of eB, but no first principle predictions are available, hence we do not infer the large field behavior.

Our work represents a preliminary investigation of the QCD critical line in a background magnetic field, which demands for further studies. There are different possible improvements to our work: for instance, we are working on a better localization, on the T, eB plane, of the critical end point, probing the transition line at values of the magnetic field interpolating between the two explored in this work. However, this goal is hard to attain because of the large lattices and the long autocorrelation times involved. Nevertheless, we are exploring more finely the critical region, trying to detect signals which permit to give a better location of the critical point. Moreover,

PoS(LATTICE2022)184

we are studying the properties of the two phases around the phase transition. On this line, we already presented our results on confinement and chirality in this paper, but we are also working on the transport properties, following Ref. [17], which could be useful in the study of heavy-ion scatterings. Further studies could be dedicated to the localization of the low-lying Dirac eigenmodes or to the glueball masses. Both of them are typical aspects of the confining quantum field theories, and studying their behavior in extreme conditions could give further information on this elusive property of QCD.

References

[1] J. O. Andersen, W. R. Naylor and A. Tranberg, Rev. Mod. Phys. **88**, 025001 (2016)

[2] V. A. Miransky and I. A. Shovkovy, Phys. Rept. **576**, 1-209 (2015)

[3] D. Grasso and H. R. Rubinstein, Phys. Rept. **348**, 163-266 (2001)

[4] V. Skokov, A. Y. Illarionov and V. Toneev, Int. J. Mod. Phys. A **24**, 5925-5932 (2009)

[5] R. C. Duncan and C. Thompson, Astrophys. J. Lett. **392**, L9 (1992)

[6] C. Bonati, M. D'Elia, M. Mariti, M. Mesiti, F. Negro and F. Sanfilippo, Phys. Rev. D **89** no.11, 114502 (2014)

[7] C. Bonati, M. D'Elia, M. Mariti, M. Mesiti, F. Negro, A. Rucci and F. Sanfilippo, Phys. Rev. D **94** no.9, 094007 (2016)

[8] C. Bonati, M. D'Elia, M. Mariti, M. Mesiti, F. Negro, A. Rucci and F. Sanfilippo, Phys. Rev. D **98** no.5, 054501 (2018)

[9] M. D'Elia, L. Maio, F. Sanfilippo and A. Stanzione, Phys. Rev. D **104** no.11, 114512 (2021)

[10] G. S. Bali, F. Bruckmann, G. Endrodi, Z. Fodor, S. D. Katz, S. Krieg, A. Schafer and K. K. Szabo, JHEP **02**, 044 (2012)

[11] G. Endrodi, JHEP **07**, 173 (2015)

[12] M. D'Elia, L. Maio, F. Sanfilippo and A. Stanzione, Phys. Rev. D **105** no.3, 034511 (2022)

[13] Y. Aoki, S. Borsanyi, S. Durr, Z. Fodor, S. D. Katz, S. Krieg et al., JHEP**06**, 088 (2009)

[14] S. Borsanyi, G. Endrodi, Z. Fodor, A. Jakovac, S. D. Katz, S. Krieg et al., JHEP**11**, 077 (2010)

[15] S. Borsanyi, Z. Fodor, C. Hoelbling, S. D. Katz, S. Krieg and K. K. Szabo, Phys. Lett. B **730**, 99-104 (2014)

[16] G. Endrodi, Z. Fodor, S. D. Katz and K. K. Szabo, JHEP **04**, 001 (2011)

[17] N. Astrakhantsev, V. V. Braguta, M. D'Elia, A. Y. Kotov, A. A. Nikolaev and F. Sanfilippo, Phys. Rev. D **102** no.5, 054516 (2020)

PoS(LATTICE2022)184